remote sensing

MDPI

Article

Decay Assessment of Stone-Built Cultural Heritage: The Case Study of the Cosenza Cathedral Façade (South Calabria, Italy)

Antonio Donato [1], Luciana Randazzo [1], Michela Ricca [1], Natalia Rovella [2], Matteo Collina [3], Nicola Ruggieri [4], Francesco Dodaro [4], Antonio Costanzo [5], Maria F. Alberghina [6], Salvatore Schiavone [6], Maria F. Buongiorno [7] and Mauro F. La Russa [1,*]

1 Department of Biology, Ecology and Earth Sciences (DiBEST), University of Calabria, 87036 Arcavacata di Rende, Italy; antonio.donato93@unical.it (A.D.); luciana.randazzo@unical.it (L.R.); michela.ricca@unical.it (M.R.)
2 Department of Biological, Geological and Environmental Sciences (BiGeA), Alma Mater Studiorum University of Bologna, 48123 Ravenna, Italy; natalia.rovella@unibo.it
3 Department of Mechanical, Energy and Management Engineering (DIMEG), University of Calabria, 87036 Arcavacata di Rende, Italy; matteo.collina@unical.it
4 Superintendence of Archeology, Fine Arts and Landscape for the Province of Cosenza, 87100 Cosenza, Italy; nicola.ruggieri@beniculturali.it (N.R.); francesco.dodaro@beniculturali.it (F.D.)
5 National Earthquake Observatory, Istituto Nazionale di Geofisica e Vulcanologia, 87036 Rende, Italy; antonio.costanzo@ingv.it
6 S.T.Art-Test, 93015 Niscemi, Italy; francesca.alberghina@gmail.com (M.F.A.); info@start-test.it (S.S.)
7 National Earthquake Observatory, Istituto Nazionale di Geofisica e Vulcanologia, 00143 Rome, Italy; fabrizia.buongiorno@ingv.it
* Correspondence: mlarussa@unical.it

Citation: Donato, A.; Randazzo, L.; Ricca, M.; Rovella, N.; Collina, M.; Ruggieri, N.; Dodaro, F.; Costanzo, A.; Alberghina, M.F.; Schiavone, S.; et al. Decay Assessment of Stone-Built Cultural Heritage: The Case Study of the Cosenza Cathedral Façade (South Calabria, Italy). *Remote Sens.* **2021**, *13*, 3925. https://doi.org/10.3390/rs13193925

Academic Editor: Devrim Akca

Received: 2 September 2021
Accepted: 27 September 2021
Published: 30 September 2021

Abstract: This study aims to assess the different decay phenomena affecting the Cosenza Cathedral façade (Calabria, South Italy) through the evaluation of the relative damage indices. For this goal, a multidisciplinary approach was applied exploiting both nondestructive and microdestructive techniques. Such a combination enabled proposing an intervention priority scale that can be helpful to institutions when planning a prompt restoration intervention. The results suggest the efficiency of this approach to obtain a multidisciplinary diagnostic and conservation system for the management and valorization of the Cultural Heritage also in terms of monitoring, maintenance, and selection of the most suitable restoration procedures over time.

Keywords: nondestructive techniques; microdestructive techniques; stone deterioration; damage indices; Cosenza; Italy

1. Introduction

The increase in weathering damage on natural stone monuments requires proper countermeasures in order to reach a sustainable monument preservation.

In this regard, in recent decades, increasing attention is being paid to the multidisciplinary approach that allows a better performance of both preventive conservation and more efficient restoration action. In order to provide a proper decay assessment of stone-built heritage and the subsequent restoration plan, a single test nondestructive technique (NDT) or microdestructive technique (MDT) may not be sufficient to provide enough data; instead, a combination of different NDTs and MDTs should be performed [1–5]. Such combination can return information on stone decay from the nanoscale to mesoscale, defining a full-scale decay assessment, which would permit dictating an intervention priority list for future restoration planning. The application of both NDTs and MDTs enables defining both quantitatively and qualitatively the different decay forms encountered and the best practice for conservation and restoration interventions.

Cosenza Cathedral is located in the old town of Cosenza (Calabria, southern Italy). It was originally built on Colle Pancrazio [6] and due to an earthquake on 9 June 1184,

it was rebuilt under Archbishop Pietro Ruffo in the current location beginning on 9 June 1185 [7]. Its rebuilding was completed by 1222 when the cathedral, according to oral tradition, was consecrated by Emperor Frederick II. During the first half of the 18th century, the church was covered by a baroque superstructure that obliterated the original structure and its works of art. In the first half of the 19th century, the façade was transformed into neogothic style, which changed completely its original aspect. At the end of the 19th century, Archbishop Camillo Sorgente entrusted the work to Pisanti, who recovered the original old arches and the ancient structure of the church. In the 1940s, the work was finally completed [8].

On 12 October 2011, the Cathedral of Cosenza received the status of UNESCO World Heritage Site for being "Heritage Witness to a Culture of Peace". This is the first award given by UNESCO to the region of Calabria [9].

This paper aims to assess the decay phenomena affecting the Cosenza Cathedral façade and the related damage indices. The alteration and degradation forms that occurred on the façade were identified in a first nondestructive phase in situ by means of macroscopical observation and preliminary InfraRed Thermography (IRT) survey. Based on these preliminary data, several in lab analyses were carried out to characterize the different decay forms encountered both qualitatively and quantitatively, such as polarizing optical microscopy (POM), ion chromatography (IC), and Fourier Transform Infrared Spectroscopy (FTIR). Data collected and integrated with Photogrammetric Survey and 3D Reconstruction were useful to define the damage indices of weathering forms, thus suggesting suitable restoration interventions.

2. Materials and Methods

The stone mainly used for building the façade of the Cathedral, as reported in the literature [10,11], was a calcarenite, a medium-grained limestone, rather soft and easy to work. The calcarenite shows a carbonate matrix that can be defined as biocalcarenite/calcirudite or biolitite/boundstone, with rare embedded clasts of igneous and metamorphic rocks, having subangular to rounded morphology. It is a porous but resistant material with a variable chromaticity ranging from whitish to reddish hues. These variations are commonly induced by a different content of ferrous minerals although other causes cannot be excluded [12,13].

A first diagnosis in situ enabled evaluation of the distribution of the different decay phenomena affecting the façade and, consequently, the choice of the samples to be taken. Five different forms were identified, following UNI 11182 [14]: black crusts, erosion/disaggregation, efflorescences, biological patina/superficial deposits, and loss of material. In this regard, a total of 43 samples (D1–D43) (Table 1) were taken from the façade at different heights above ground level (Figure 1).

Table 1. Brief description of samples taken with respective sampling point and analysis. Macroscopic features of investigated samples together with the sampling point according to Figure 1 and employed techniques on each sample. CLC = Fragment of calcarenite; D-CLC = Disaggregated calcarenite; EF = Effloresecences; SEF = Subefflorescences; BSL = Blackish superficial layer; GSL = Greyish superficial layer; U = Unaltered; IC = Ion Chromatography; FT-IR = Fourier transform infrared spectroscopy; POM = polarizing microscope.

Sample ID	Description	Height above Ground (m)	Employed Techniques
D1	CLC, U	1.1	IC
D2	CLC, GSL	1.1	IC

Table 1. *Cont.*

Sample ID	Description	Height above Ground (m)	Employed Techniques
D3	CLC, GSL	2.3	POM
D4	CLC, GSL	1.4	FTIR
D5	EF	2.2	IC, FTIR
D6	D-CLC	1.8	IC
D7	CLC, U	3.0	FTIR
D8	CLC, BSL	1.6	POM
D9	CLC, U	2.6	IC, FTIR
D10	CLC, U	1.9	FTIR
D11	D-CLC, EF-SEF	2.3	IC, FTIR
D12	CLC, U	1.2	FTIR
D13	CLC, BSL	5.9	POM
D14	D-CLC, BSL	4.6	IC, FTIR
D15	D-CLC, BSL	4.8	IC, FTIR
D16	D-CLC	4.9	IC
D17	CLC, U	5.0	IC
D18	D-CLC	5.4	IC, FTIR
D19	D-CLC	5.5	IC, FTIR
D20	D-CLC, BSL	5.5	IC, FTIR
D21	CLC, BSL	7.6	POM
D22	CLC, GSL	7.3	FTIR
D23	CLC, BSL	7.5	POM
D24	CLC, BSL	7.8	FTIR
D25	CLC, BSL	8.1	FTIR
D26	CLC, GSL	9.0	FTIR
D27	CLC, U	9.2	FTIR
D28	CLC, GSL	9.3	POM
D29	CLC, U	4.3	FTIR
D30	D-CLC, BSL	4.1	FTIR
D31	CLC, BSL	4.0	POM
D32	CLC, GSL	4.0	FTIR
D33	CLC, BSL	4.1	FTIR
D34	D-CLC, BSL	7.8	IC
D35	CLC, BSL	7.2	FTIR
D36	CLC, BSL	7.7	FTIR
D37	CLC, BSL	8.2	POM
D38	CLC, BSL	8.9	POM
D39	D-CLC, BSL	7.5	IC, FTIR
D40	D-CLC, BSL	8.3	IC, FTIR
D41	CLC, BSL	15.0	FTIR
D42	CLC, GSL	14.4	FTIR
D43	CLC, BSL	22.4	POM

Next, the samples were analyzed via POM, IC and FTIR, in order to characterize qualitatively and quantitatively the different decay forms encountered. Subsequently, their detailed mapping and damage analysis were realized carrying out a photogrammetric survey (Figure 2).

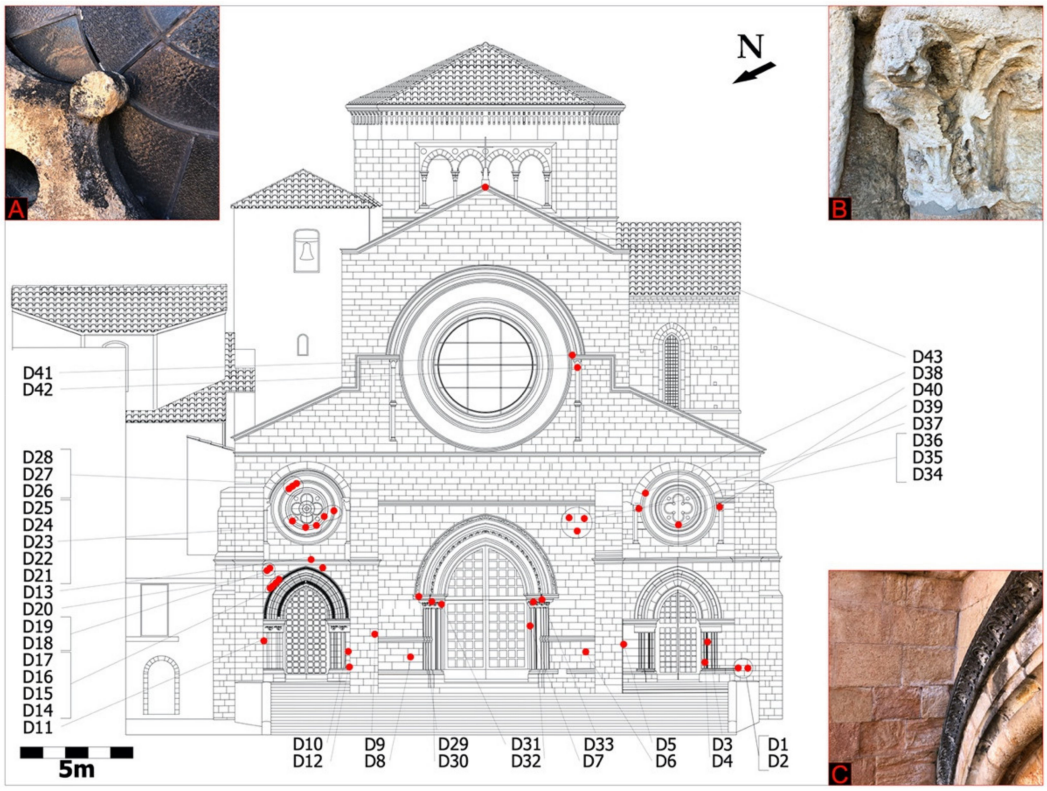

Figure 1. Samples taken from the façade. The images show some deteriorated areas in detail and relevant samples: (**A**) D21-D22; (**B**) D32-D33; and (**C**) D14-D15-D16-D17.

Figure 2. Workflow of the process carried out.

2.1. IR Thermography

Infrared thermography (IRT) is a nondestructive technique widely employed in the analysis of Cultural Heritage (CH) [15,16]. In fact, IRT represents a fundamental tool in the CH diagnostic field for conservation state assessment thanks to the possibility of determining the temperature of a surface by measuring the IR radiation emitted by each object as a function of the temperature, T (°C). This technique is useful, for example, in the detection of superficial cracks, detachments, material differences, or moisture presence within structures. Indeed, the compositional or structural inhomogeneities, at or below the investigated surface, locally affect the homogeneous heat propagation and result in thermal contrast in the thermogram.

The main features investigated by the IRT technique in the monumental heritage were: (*i*) the state of conservation of architectural structures, the wall texture hidden under plaster layers, any architectural changes or additions to the original one (for example, window and door cladding); (*ii*) the quality of thermal insulation; (*iii*) the conservation state of plasters or pictorial layers, their adhesion to the support layer, the mapping of detachments or defects in the plaster, as well the identification of the different building materials due to their different emissivity value; (*iv*) moisture, water infiltrations, or dispersions, even inside the masonry whose degradation effects are not yet visible on the surface.

In the present case, a FLIR model B335 thermal imaging camera equipped with an uncooled microbolometric thermal sensor (320 × 240 pixel resolution, from −20 °C to +120 °C thermal range, +/− 2% of the detected temperature accuracy; 7.5 ÷ 13 μm spectral range; 1.36 mrad spatial resolution; embraced field 25° × 19°) was used. The camera was also equipped with a 3.1 Mpixel photographic sensor that allowed the acquisition of the thermal image at the same time as the visible one, with the same shooting conditions.

The IRT investigation was performed without induced artificial warming of the surfaces, acquiring the data under different climatic conditions in order to take advantage of the natural heat exchange between the structure and the environment. For this reason, the thermal anomalies were documented on different days during the survey period (February and March 2021) and the temperature and relative humidity values were recorded (Table 2). Moreover, the thermographic images were processed and calibrated also considering the specific thermohygrometric values measured at the moment of investigation.

Table 2. Temperature (T °C medium, T °C min, and T °C max) and relative humidity (RH% medium) values measured for each February and March 2021 days on which the IR thermography investigation was carried out.

Day	T °C (medium)	T °C (min)	T °C (max)	RH% (medium)
February 22	13 °C	10 °C	18 °C	76%
February 23	13 °C	7 °C	17 °C	78%
February 24	12 °C	7 °C	16 °C	83%
March 3	10 °C	4 °C	16 °C	65%
March 4	9 °C	2 °C	15 °C	81%
March 5	10 °C	2 °C	15 °C	79%

Generally, all IR thermograms could be affected by the dependence of the emissivity on the shooting angle. Then each sample area was documented through different angles, in order to guarantee the significance of the detected thermal anomalies (attributable to moisture, detachments, fractures, different materials), excluding artifacts due to the setting conditions.

2.2. Photogrammetric Survey and 3D Reconstruction

The most widespread application of photogrammetry concerns the representation of the facades or elevations of historic buildings and structure. By improving digital techniques, digital close-range photogrammetry has become a more efficient and more

economic method. Obtained 3D solid or textured images help to understand sophisticated and complex buildings more easily.

One of the most important advantages of using digital close-range photogrammetry to supply documentation is in measuring dangerous or inaccessible areas, very high or low buildings, or part of these buildings. It represents an important support in obtaining the required measurement of the parts of the building from the photograph [17].

2.3. Damage Analysis

Evaluation, quantification, and rating of stone damages via monument mapping is based on objective description and registration, according to type and intensity, of weathering forms [18]. The preliminary in situ diagnosis and the photogrammetric survey enable exact location of all weathering forms affecting the façade.

While such forms are involved in the definition of deterioration phenomena according to type and intensity, damage categories and damage indices have been established as a practical tool for the rating of damage and as a contribution to risk prognosis and risk management. According to defined schemes, all weathering forms (considering different intensities) are related to damage categories [19].

Damage indices are calculated from damage categories (differentiated by area percentage; interested area over total area). Linear and progressive damage indices are defined as:

$$DI_{lin} = [(A \times 0) + (B \times 1) + (C \times 2) + (D \times 3) + (E \times 4) + (F \times 5)] \quad (1)$$

$$DI_{prog} = \sqrt{(((A \times 0^2) + (B \times 1^2) + (C \times 2^2) + (D \times 3^2) + (E \times 4^2) + (F \times 5^2))/100)} \quad (2)$$

where each letter (A–F) represents the sum of percentage area of different decay forms referred to the same damage category (0–5).

Damage indices range from 0 to 5.0. According to the defined calculation modes, the linear damage index corresponds to the average damage category, whereas the progressive damage index emphasizes proportion of the higher damage categories. The difference between those indices increases as the proportion of higher damage categories increases.

2.4. Polarizing Optical Microscopy

Polarizing optical microscopy (POM) was applied to identify the main minero-petrographic features of the stone and to characterize the superficial layers, preparing thus stratigraphic thin sections. Moreover, it was possible to obtain information about the interaction between the altered superficial layer and the substrate.

POM was performed using a Zeiss AxioLab microscope (Oberkochen, Germany) equipped with a digital camera to capture images.

Out of a total of 43 samples, 10 were selected because they were considered the most representative of the main observed degradation forms (Table 1).

2.5. Ion Chromatography and Fourier Transform Infrared Spectroscopy

The combined performance of IC and FTIR provide a quantitative and qualitative characterization of the different samples analyzed ([20] and references therein). Due to the complementarity of these two kinds of analysis, their results will be discussed together.

Ion chromatography is a method that enables determination of the concentrations of analytes in an unknown sample [21].

A Dionex DX 120 equipment on filtered supernatant (filter Minisart RC 25, diameter = 0.45 µm) provided ion-chromatography data both on untreated and treated samples, determining ionic species such as SO_4^{2-}, NO_3^-, Cl^-, F^-, Br^-, Li^+, NH_4^+, Na^+, K^+, Ca^{2+}, and Mg^{2+}.

Fourier Transform Infrared Spectroscopy (FTIR) is an analytical technique able to identify organic, polymeric, and inorganic materials. The FTIR analysis method uses infrared light to scan test samples and observe chemical properties [22].

The infrared spectra were collected with a spectrophotometer Perkin Elmer Spectrum 100 (Waltham, MA, USA), equipped with an attenuated total reflectance (ATR). The ATR accessory is equipped with a diamond crystal, in the range 500–4000 cm^{-1} at a resolution of 4 cm^{-1}.

The technique was used to analyze small amounts of black crust and/or efflorescence samples drawn from samples surfaces using a scalpel.

3. Results

3.1. IR Thermography

The IRT investigation was carried out on the wall structures and the architectural decorative elements of the main façade of the Cathedral, both the external and internal side.

The acquired IR thermograms made it possible:

- to map the different materials relating to the changes in the architectural system verifying the known historical information about the several restorations that the building has undergone in the past;
- to quickly assess the presence of thermal discontinuities attributable to efflorescence degradation, moisture, and physical damage on the stone surfaces of the façade.

In particular, at the lower parts of the external side, thermal anomalies associated with capillary rising phenomena were observed.

In the upper part, thermal anomalies compromising the structural proprieties and aesthetic values of the wall structures of the façade were detected. As clearly revealed in Figure 3, indeed, at the height of the lateral rose window, a wide water infiltration affects a large part of the façade.

Figure 3. Thermograms acquired on the external side (**a**) and on the corresponding internal side (**b**) and comparison with the photographic images of the same areas investigated. The colder areas (blue tones) locate the infiltration at the height of the side rose. A temperature of 12.7 °C and 64% relative humidity values measured during the 23 February 2021 in situ morning session were used to postprocess the thermograms here reported. This portion of the facade of the cathedral is related to an infiltration of rainwater from the external side of the masonry or from the roof and extends up to the frames of the rose window.

Correspondingly, on the internal side, the IRT inspection documented the higher intensity signal due to a presence of rainwater in the same portion of the wall structure. The diagnostic evidence confirmed that the rainwater infiltration through damage to the roofing system is one of the causes of the major deterioration in this wall portion.

The water migration into the porosity of the stone blocks due to evaporative phenomena led to the formation of salts efflorescence on the external side and, consequently, induced an important superficial decohesion, also identifiable in IRT images as colder surfaces.

3.2. Photogrammetric Survey and 3D Reconstruction

The 3D model can be helpful to evaluate the structures in their entirety, their conservation state and, moreover, to recognize and evaluate the distribution and the evolution of the different degradation processes characterized during the laboratory analysis. In fact, 3D imaging techniques associated with photographic documentation grant a high level of detail, making the identification of interested areas easier and more efficient as well as the assessment of damage indices.

The photogrammetric survey was carried out by a drone (Figure 4) and the subsequent data processing was realized by software as Meshlab (www.meshlab.net accessed on 15 July 2021), to generate a 3D mesh, and AutoCAD, to estimate the degraded areas.

Figure 4. Detail of photogrammetric survey.

AutoCAD software enabled association of each decay form to a single hatch; whereas the calculation of the areas was performed by AutoCAD simultaneous with the hatch creation.

The mapping of the area with individual forms of decay (previously identified), and their extensions, is reported below (Table 3, Figure 5).

Table 3. Weathering forms areas.

	Black Crusts	Erosion/ Disaggrega-tion	Efflorescences	Biological Patina/Superficial Deposits	Loss of Material
Area (cm^2)	198,328.5	481,235.3	51,506.3	471,502.5	31,402.5
Area (%)	5.75	13.95	1.49	2.29	0.91

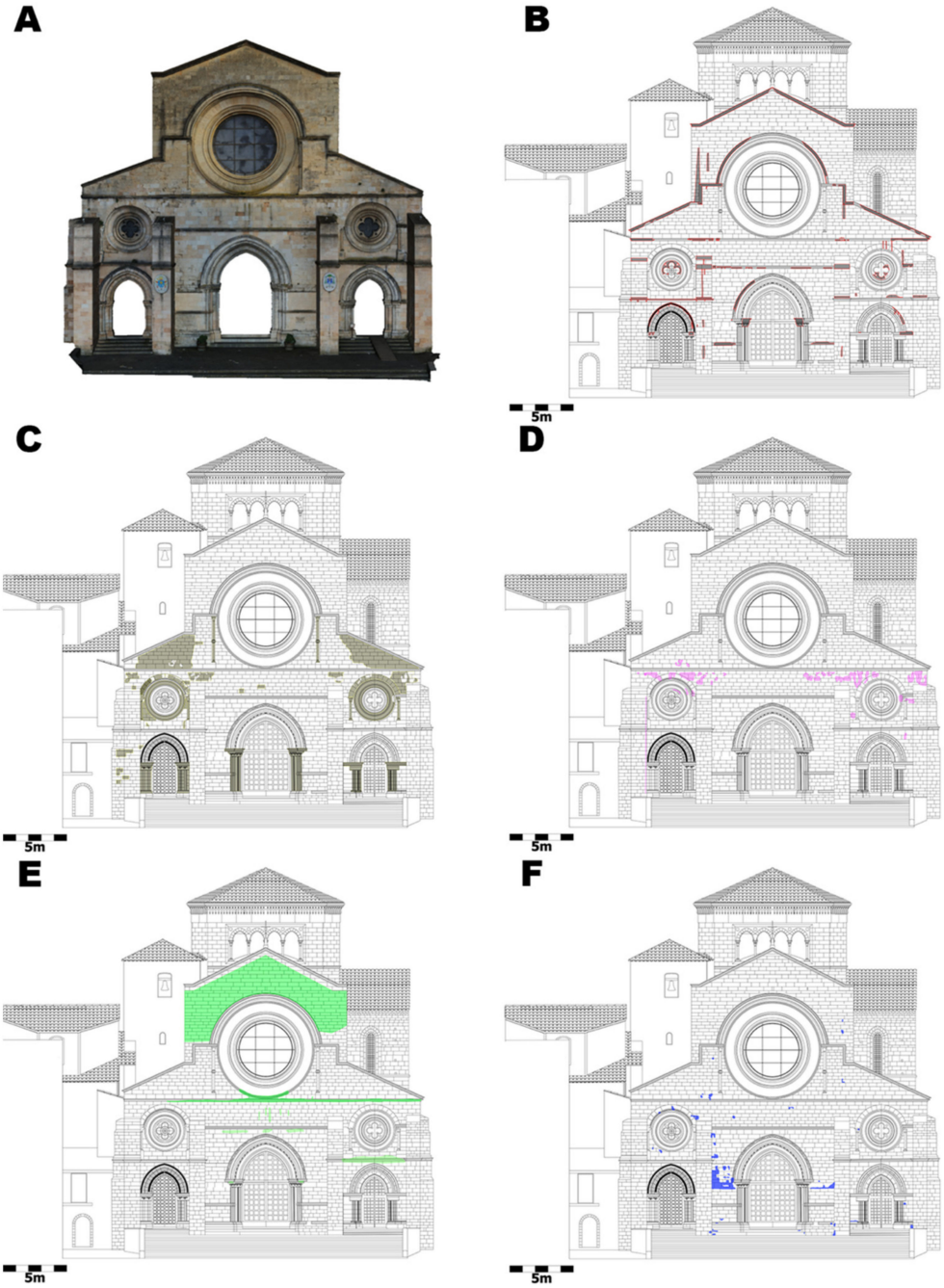

Figure 5. (**A**) 3D model of the façade; (**B**) Black crust; (**C**) Erosion/Disaggregation; (**D**) Efflorescences; (**E**) Biological patina/Superficial deposits; (**F**) Loss of material.

3.3. Damage Analysis

Damage categories were attributed to previously mentioned forms in order to calculate the linear and progressive damage indices (Table 4). Damage categories values were evaluated as an average over the whole façade.

Table 4. Damage index evaluation.

Weathering Forms	Parameters Considered during Evaluation						
Black crusts	Intensity	Cover degree of the surface (%)					
		<15	25	50	75	100	
	Damage category	0	1	2	3	4	5
Erosion/ Disaggregation		Depth (mm and/or cm)					
	Intensity	<0.5	0.5–1	1–3	3–5	5–10	10–25
	Damage category	0	1	2	3	4	5
Efflorescences		Cover degree of the surface (%)–Color change degree					
	Intensity	<10	25	50	75	100	
		Chromatic alteration			Whitening		
	Damage category	0	1	2	3	4	5
Biological patina/ Superficial deposits		Cover degree of the surface (%)					
	Intensity	<10	25	50	75	100	
	Damage category	0	1	2	3	4	5
Loss of material		Cover degree of the surface (%)					
	Intensity	<10	25	50	75	100	
	Damage category	0	1	2	3	4	5

Damage indices obtained for the entire façade were equal to:

$$DI_{lin} = 0.86 \quad (3)$$

$$DI_{prog} = 1.66 \quad (4)$$

The difference between progressive and linear indices is an indication of how much the decay forms belonging to higher damage category (efflorescences and erosion in this case) weigh on the indices' calculations.

As highlighted during in situ decay observations, the left side of the façade was mostly affected by both efflorescences and erosion phenomena; therefore, damage indices were determined also on the two portions of the façade (left and right). The damage indices of the two portions were respectively: DI_{lin} = 1.06 and DI_{prog} = 2.06 for the left side, DI_{lin} = 0.67 and DI_{prog} = 1.27 for the right side. They suggest the necessity to intervene urgently in this area with a restoration plan.

3.4. Polarizing Optical Microscopy

Petrographic observations suggest how all samples show similar features; in particular, they can be classified as biosparites/biopelsparites (Folk classification [23]) or wackestone (Dunham classification [24]). The most abundant accessory clasts were mostly siliciclastics, as quartz, plagioclase, micas (biotite, muscovite), and polycrystalline quartz. Fragments of granitoid rocks were found in D13 and D21 thin sections (Figure 6).

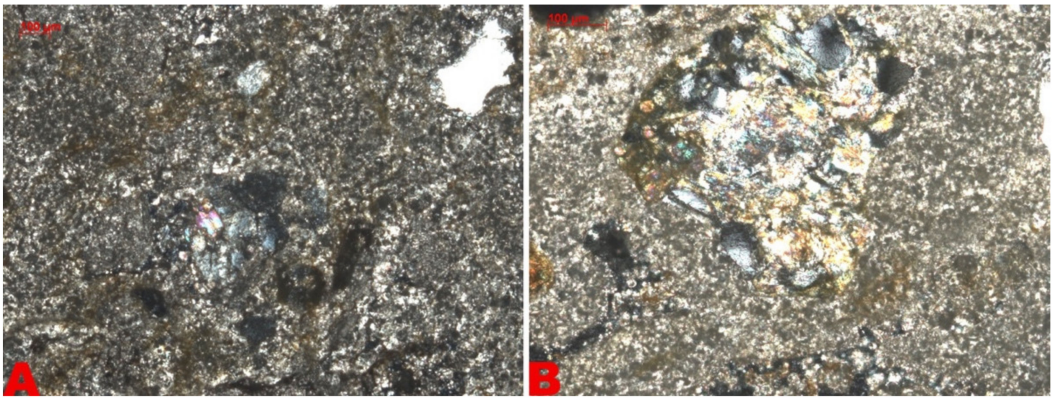

Figure 6. Fragments of granitoid in D13 (**A**) and D21 (**B**) samples (crossed polarized light view, CPL).

The samples appear to be compact, with the exception of D21, D23, D28, and D31 where a slight fracturation was detected, with a secondary porosity <20%.

A superficial layer with variable thickness, made of microcrystalline gypsum, was observed on D13, D23, D31, D37, and D43 specimens. The level was related to the degradation forms (black crusts) identified under macroscopic observation. Traces of *scialbatura* (i.e. a sort of thin finishing lime layer) were found in D28 and D38 thin sections (Figure 7A,B).

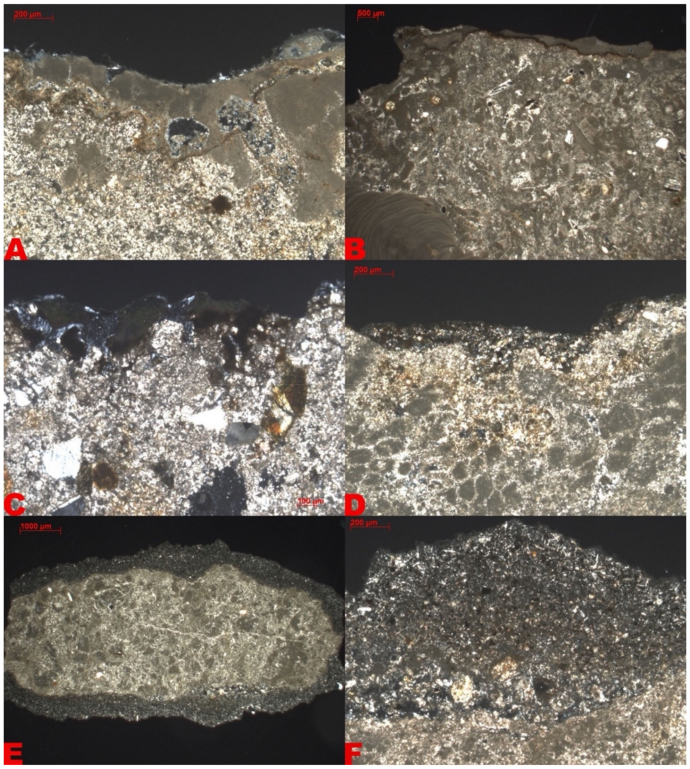

Figure 7. (**A**,**B**) *Scialbatura* traces in D28 and D38 thin sections; (**C**) Siliciclastic accessory clasts mainly encountered; (**D**) Superficial layer overlying the substrate in D31 sample; (**E**,**F**) D37 sample and detail of the overlying black crust with visible acicular crystals of gypsum, Fe-oxides, and carbonaceous particles.

The superficial layer was discontinuous in most of the samples, with an average thickness ranging from 120 µm to 265 µm. It showed an irregular lower profile, while the upper one varied from irregular to lobate (Figure 7C,D). D37 was the only sample in which the superficial layer showed different characteristics. It appeared to continue in

the whole sample, with a thickness ranging from 350 to 900 µm. The crust was adherent to the substrate, except in some parts where it was fractured. The superficial layer was constituted mainly of microcrystalline gypsum; in addition, it was possible to observe also acicular gypsum crystals, Fe-oxides, and carbonaceous particles (Figure 7E,F).

3.5. Ion Chromatography and Fourier Transform Infrared Spectroscopy

IC analysis showed most of the samples were characterized by a high amount of sulphate and carbonate, associated with sodium and calcium (Table 5, Figure 8).

Table 5. Anions and cations concentrations (mg/L).

Sample ID	Li^+	Na^+	NH_4^+	K^+	Mg^{2+}	Ca^{2+}	Sr^{2+}	F^-	Cl^-	HCO_3^-	Br^-	NO_3^-	PO_4^{3-}	SO_4^{2-}
D1	0.0	3.4	0.1	1.4	2.5	10.3	0.2	0.3	2.0	19.8	0.0	2.8	0.0	12.7
D2	0.0	3.4	0.0	2.5	1.8	29.1	0.0	0.2	1.5	21.4	0.0	9.6	0.0	62.4
D5	0.0	106.1	0.0	17.0	0.2	1.8	0.0	0.1	2.7	230.3	0.0	23.0	0.0	74.4
D6	0.0	2.9	0.0	1.0	1.6	6.7	0.0	0.0	2.2	25.9	0.0	6.7	0.0	3.9
D9	0.0	3.6	0.1	1.1	2.1	35.8	0.0	0.1	2.5	16.8	0.0	4.4	0.0	81.0
D11	0.0	53.2	0.0	0.8	0.4	1.6	0.0	0.2	0.5	172.4	0.0	0.9	0.5	20.0
D14	0.0	2.5	0.0	0.3	1.3	107.3	0.6	0.1	0.6	18.3	0.0	1.5	0.0	289.3
D15	0.0	1.8	0.2	0.3	1.5	144.0	1.4	0.5	0.3	29.0	0.0	0.3	0.0	308.3
D16	0.0	0.7	0.1	0.3	1.9	7.0	0.0	0.4	0.3	32.0	0.0	0.2	0.0	5.2
D17	0.0	2.3	0.0	0.4	1.8	5.8	0.0	0.1	0.2	36.6	0.0	0.3	0.0	1.7
D18	0.0	56.7	0.0	1.1	0.6	2.6	0.0	0.1	0.9	152.5	0.0	2.6	0.0	17.4
D19	0.0	47.0	0.0	1.0	0.5	2.3	0.0	0.1	2.2	128.1	0.0	6.4	0.0	14.4
D20	0.0	2.7	0.1	0.6	2.1	58.6	0.0	0.1	2.4	45.8	0.0	2.0	0.0	131.6
D34	0.0	2.1	0.2	0.6	6.2	11.3	0.0	0.5	1.3	67.1	0.0	5.1	0.0	6.6
D39	0.0	1.2	0.1	0.4	1.3	86.7	0.9	1.2	0.8	38.1	0.0	1.6	0.0	224.8
D40	0.0	1.3	0.0	0.4	1.9	74.7	0.0	0.3	0.9	42.7	0.0	0.6	0.0	182.3

From the study of vibrational bands via FTIR, many mineralogical phases were identified, such as gypsum and calcite (Figure 9); moreover, traces of silicates were found (Table 6).

The presence of calcite can be attributed to the carbonate substrate while the presence of gypsum may depend on sulfation reactions caused by polluting agents, associated with black crust and efflorescence genesis.

The IC results showed a good correlation between calcium and sulphate, testifying, according to FTIR analysis, that these two species were mainly present in the form of gypsum. The same behavior could not be determined for sodium and chlorine. In fact, an excess of sodium was evident in all samples compared to chlorine. This may be due to the presence of sodium sulphates as well as sodium chloride. As is well known, the presence and the crystallization of these soluble salts from repeated cycles of crystallization/dissolution within the porous matrix of the stone in porous materials is one of the major causes of rock decay in nature [25] and weathering of natural and/or artificial building material [26–28]. The growth of a crystal in a confined space (pore) can alter both the porosity and the pore size distribution of the stones, changing also their mechanical properties [29]. This process is emphasized in some sulphate species, particularly sodium sulphate. It exerts crystallization pressures on the pore walls, and in addition, undergoes a change in volume during its transition to the hydrated form (mirabilite), producing also a certain hydration pressure. The data collected in Table 4, report the largest concentration of these sodium sulphates in D5, D11, D18, and D19 coming from the portion of the church façade where efflorescences were much more intense. These samples also showed the highest rate of disintegration and fracturing, confirming the damaging effect of salt crystallization.

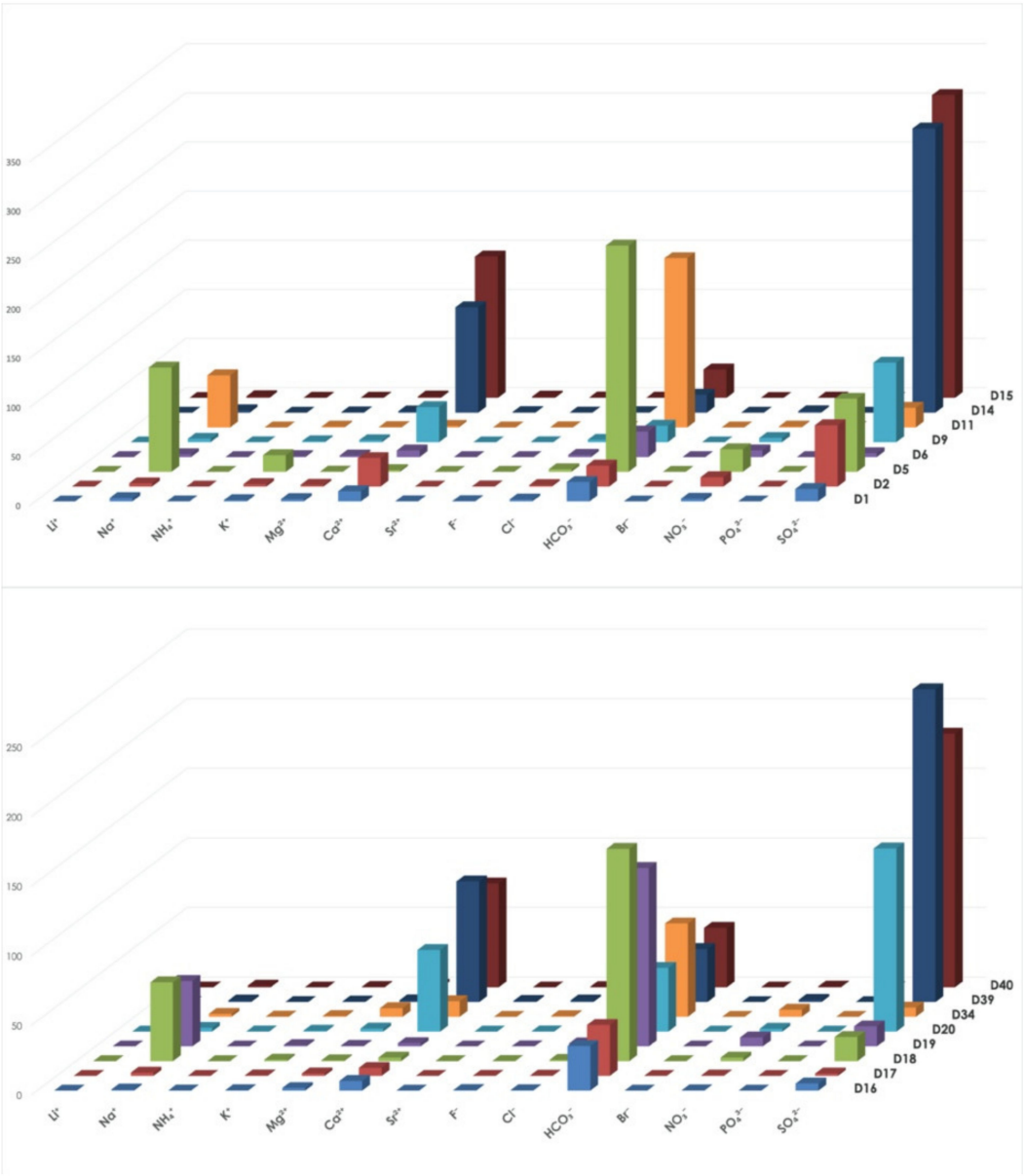

Figure 8. Anion and cation concentrations (mg/L).

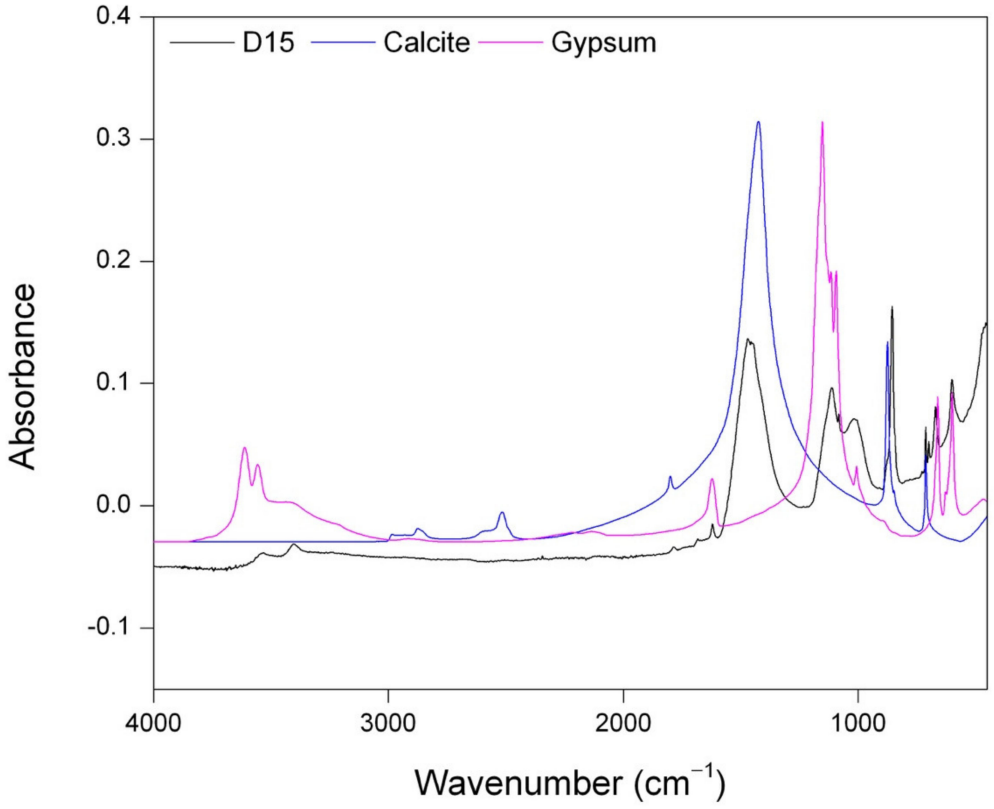

Figure 9. D15 sample IR spectra.

Table 6. Vibrational bands (wavenumber cm^{-1}) of the different mineralogical phases identified.

Sample ID	Calcite	Gypsum	Silicates
D4	1429, 879, 729		1646, 1167, 1082, 781
D7	1429, 877, 729		1646, 1085, 781
D9	1440, 878, 729	3546, 3403, 1621, 671, 609	1679, 1140, 1119
D10	1434, 877, 727		1022, 1084, 781
D11	1404, 875, 713		1661, 1082, 1016
D12	1435, 877, 727	3551, 3410, 1621, 661, 600	1623, 1082, 1038
D14	1458, 856, 713	3541, 1622, 1109, 1009, 670, 596	
D15	1779, 1447, 855, 714	3531, 3407, 1621, 1113, 1084, 1010, 670, 601	
D18	1403, 874, 713	3453, 1654, 648, 615	1790, 1082, 692
D19	104, 873, 714	3351, 1656, 649, 614	1790, 1081, 693
D20	1787, 1447, 874, 713	3542, 1622,1116, 1084, 670, 601	1083, 782, 700
D22	1804, 1435, 878, 730		1652, 1080, 1031, 781
D24	1788, 1427, 878, 729		1640, 1083, 1031, 783
D27	1808, 1417, 876, 728		1645, 1031, 784, 665
D29	1800, 1417, 873,7 13	3554, 1621, 1121, 669, 602	1667, 1083, 783
D30	1791, 1415, 875, 713	3410, 1641, 607	1788, 1082, 698
D35	1793, 1417, 874, 713		1647, 1008
D39	1787, 1446, 855, 713	3542, 1621, 1116, 1093, 670, 600	
D40	1785, 1446, 879, 710	3541, 3400, 1621, 1112, 1082, 671, 607	

4. Discussion

The use of nondestructive techniques such as IRT and photogrammetric survey provided helpful data to define the areas of major interest that needed further investigation and to be sampled. The results of the temperature behavior of the stone materials can contribute to the characterization of stone types, weathering state and damage, and exposition settings. Moreover, such results can also indicate areas which are affected by high humidity load (e.g., façade left part).

The combination of those techniques was crucial in terms of efficiency and time-consuming analysis as both techniques are quite quick to execute. Reducing time for diagnosis enables producing a faster response for institutions when planning a prompt restoration intervention.

Following a priority scale provided by damage categories assigned to different weathering forms, it would be recommendable to intervene firstly on areas affected by efflorescences, paying attention to the area above the left portal of the façade; while erosion covers about 14% of the façade, efflorescences may exacerbate the strong erosion already present and the combined effect of those may compromise the conservation of the whole structure. Although the area above the right portal of the façade has efflorescences, they are less intense; the uneven progression between these parts could be due to a heavy water infiltration on the left part, as highlighted by IRT, which favored its evolution over time. Finally, a cleaning intervention is required on areas affected by black crusts and biological patina.

5. Conclusions

The diagnostic phase carried out in situ combined with the results of in lab analysis and the integration with the 3D model demonstrated the efficiency of this multidisciplinary approach in the assessment of the conservation state of built heritage and in the planning of the restoration interventions.

Nondestructive techniques enabled characterization of the damage on the façade on a mesoscale, while microdestructive techniques from nano to microscale, provided a complete decay assessment of the case study and the subsequent intervention priority scale.

This survey may represent a good practice to develop a damage diagnosis, leading to important practical concerns for an acceptable decision-making process to be applied in future restoration of stone-built heritage. In this regard, the results will be later integrated into an information system, available in realtime, allowing institutions to monitor its conservative status over time.

Author Contributions: Conceptualization, M.F.L.R., N.R. (Nicola Ruggieri) and F.D.; formal analysis, A.D., M.R., L.R., N.R. (Natalia Rovella), M.F.A. and S.S.; investigation, A.D., M.R., L.R., N.R. (Natalia Rovella), M.C., M.F.A. and S.S.; writing—original draft preparation, A.D., M.R., L.R., N.R. (Natalia Rovella), M.F.A. and S.S.; writing—review and editing, A.D., M.R., L.R., N.R. (Natalia Rovella), M.F.A. and S.S.; visualization, A.D.; supervision, M.F.L.R., A.C., M.F.B.; funding acquisition: M.F.L.R., A.C., M.F.B. All authors have read and agreed to the published version of the manuscript.

Funding: The research activities have been partially funded by the project "ARCH—Advancing Resilience of historic areas against Climate-related and other Hazards" in the framework of the European Union's Horizon 2020 research and innovation programme under grant agreement no. 820999. The sole responsibility for the content of this publication lies with the authors. It does not necessarily represent the opinion of the European Union. Neither the European Research Executive Agency (REA) nor the European Commission are responsible for any use that may be made of the information contained therein.

Institutional Review Board Statement: Not applicable.

Informed Consent Statement: Not applicable.

Data Availability Statement: Not applicable.

Acknowledgments: We thank the three anonymous reviewers for their careful reading and helpful suggestions.

Conflicts of Interest: The authors declare no conflict of interest.

References

1. Diz-Mellado, E.; Mascort-Albea, E.J.; Romero-Hernández, R.; Galán-Marín, C.; Rivera-Gómez, C.; Ruiz-Jaramillo, J.; Jaramillo-Morilla, A. Non-destructive testing and Finite Element Method integrated procedure for heritage diagnosis: The Seville Cathedral case study. *J. Build. Eng.* **2021**, *37*, 102134. [CrossRef]
2. Chastre, C.; Ludovico-Marques, M. Chapter 13—Nondestructive testing methodology to assess the conservation of historic stone buildings and monuments. In *Handbook of Materials Failure Analysis*; Makhlouf, A.S.H., Aliofkhazraei, M., Eds.; Butterworth-Heinemann: Oxford, UK, 2018; pp. 255–294. [CrossRef]
3. Kilic, G. Using advanced NDT for historic buildings: Towards an integrated multidisciplinary health assessment strategy. *J. Cult. Herit.* **2015**, *16*, 526–535. [CrossRef]
4. Bosiljkov, V.; Uranjek, M.; Žarnić, R.; Bokan-Bosiljkov, V. An integrated diagnostic approach for the assessment of historic masonry structures. *J. Cult. Herit.* **2010**, *11*, 239–249. [CrossRef]
5. Bosiljkov, V.; Maierhofer, C.; Koepp, C.; Wöstmann, J. Assessment of Structure through Non-Destructive Tests (NDT) and Minor Destructive Tests (MDT) Investigation: Case Study of the Church at Carthusian Monastery at Žiče (SLOVENIA). *Int. J. Archit. Herit.* **2010**, *4*, 1–15. [CrossRef]
6. Andreotti, D. *Storia dei Cosentini*, 1st ed.; Pellegrini: Cosenza, Italy, 1978; Volume 1.
7. Rubino, G.E.; Teti, M.A. Cosenza. Le Città Nella Storia d'Italia, 1st ed.Laterza: Roma, Italy, 1997.
8. Mascioni Organs. Available online: https://www.mascioni-organs.com/en/cosenza-italy-cathedral/ (accessed on 15 July 2021).
9. Your Italy. Available online: https://www.youritaly.it/en/guides/calabria/the-city-of-cosenza (accessed on 15 July 2021).
10. Crisci, G.M.; De Francesco, A.M.; Gattuso, C.; Miriello, D. Un metodo geochimico per la determinazione della provenienza di lapidei macroscopicamente omogenei. Un esempio di applicazione sui monumenti del centro storico di Cosenza. *Arkos Sci. Restaur. Archit.* **2012**, *2*, 52–59.
11. Mastrandrea, A.; Muto, F.; Neri, C.; Papazzoni, C.A.; Perri, E.; Russo, F. Deep-Water Coral Banks: An Example from the "Calcare di Mendicino" (Upper Miocene, Nothern Calabria, Italy). *Facies* **2012**, *47*, 27–42. [CrossRef]
12. Randazzo, L.; Collina, M.; Ricca, M.; Barbieri, L.; Bruno, F.; Arcudi, A.; La Russa, M. Damage Indices and Photogrammetry for Decay Assessment of Stone-Built Cultural Heritage: The Case Study of the San Domenico Church Main Entrance Portal (South Calabria, Italy). *Sustainability* **2020**, *12*, 5198. [CrossRef]
13. Ricca, M.; Le Pera, E.; Licchelli, M.; Macchia, A.; Malagodi, M.; Randazzo, L.; Rovella, N.; Ruffolo, S.; Weththimuni, M.; La Russa, M. The CRATI Project: New Insights on the Consolidation of Salt Weathered Stone and the Case Study of San Domenico Church in Cosenza (South Calabria, Italy). *Coatings* **2019**, *9*, 330. [CrossRef]
14. UNI 11182. *Cultural Heritage. Natural and Artificial Stone. Description of the Alteration—Terminology and Definition*; Ente Nazionale Italiano di Unificazione (UNI): Milan, Italy, 2006.
15. Mercuri, F.; Cicero, C.; Orazi, N.; Paoloni, S.; Marinelli, M.; Zammit, U. Infrared Thermography Applied to the Study of Cultural Heritage. *Int. J. Thermophys.* **2015**, *36*, 1189–1194. [CrossRef]
16. Moropoulou, A.; Avdelidis, N.P.; Karoglou, M.; Delegou, E.T.; Alexakis, E.; Keramidas, V. Multispectral Applications of Infrared Thermography in the Diagnosis and Protection of Built Cultural Heritage. *Appl. Sci.* **2018**, *8*, 284. [CrossRef]
17. Yilmaz, H.M.; Yakar, M.; Gulec, S.A.; Dulgerler, O.N. Importance of digital close-range photogrammetry in documentation of cultural heritage. *J. Cult. Herit.* **2007**, *8*, 428–433. [CrossRef]
18. Fitzner, B.; Heinrichs, K. Damage diagnosis at stone monuments—Weathering forms, damage categories and damage indices. *Underst. Manag. Stone Decay.* **2001**, *45*, 1–49.
19. Fitzner, B.; Hinrichs, K.; La Bouchardiere, D. Damage Index for Stone Monuments. In *Protection and Conservation of the Cultural Heritage of the Mediterranean Cities, Proceedings of the 5th International Symposium on the Conservation of Monuments in the Mediterranean Basin, Sevilla, Spain, 5–8 April 2000*; Swets, Zeitlinger: Lisse, The Netherlands, 2000.
20. Montana, G.; Randazzo, L.; Mazzoleni, P. Natural and anthropogenic sources of total suspended particulate and their contribution to the formation of black crusts on building stone materials of Catania (Sicily). *Environ. Earth Sci.* **2012**, *67*, 1097–1110. [CrossRef]
21. OSU Chemistry REEL Program. Available online: https://research.cbc.osu.edu/reel/research-modules/environmental-chemistry/instrumentation/instrument-calibration/ion-chromatography-theory/ (accessed on 15 July 2021).
22. RTI Laboratories. Available online: https://rtilab.com/techniques/ftir-analysis/ (accessed on 15 July 2021).
23. Folk, R.L. Spectral subdivision of limestone types. *Bull. Am. Assoc. Pet. Geol.* **1962**, *1*, 62–84.
24. Dunham, R.J. Classification of Carbonate Rocks According to Depositional Textures. *Amer. Ass. Pet. Geol.* **1962**, 108–121.
25. Evans, I.S. Salt crystallization and rock weathering: A review. *Rev. Géomorphol. Dyn.* **1970**, *19*, 153–177.
26. Winkler, E.M. *Stone in Architectur*, 1st ed.; Springer: Berlin/Heidelberg, Germany, 1994.

27. Goudie, A.S.; Viles, H.A. *Salt Weathering Hazard*, 1st ed.; Wiley: London, UK, 1997.
28. Rodriguez-Navarro, C.; Doehne, E. Salt weathering: Influence of evaporation rate, supersaturation and crystallization pattern. *Earth Surf. Process. Landf.* **1999**, *24*, 191–209. [CrossRef]
29. Dei, L.M.; Mauro, M.; Baglioni, P.; Del Fa, C.M.; Fratini, F. Growth of crystal phases in porous media. *Langmuir* **1999**, *15*, 8915–8922. [CrossRef]